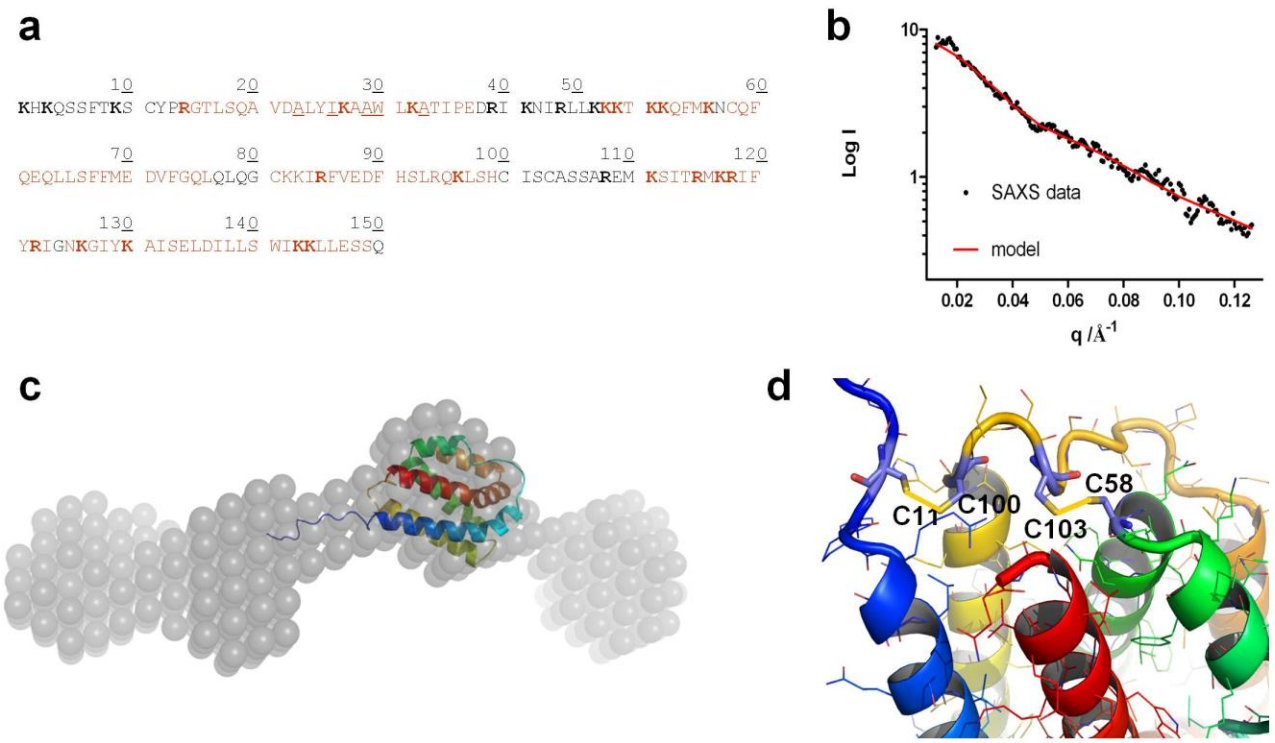


Supplementary Figure 1

**Structural characterization of IL-26.**

(**a**) Amino acid sequence of IL-26. Amino acids within the 6 predicted α-helical regions are labeled in red. Positively charged amino acids clustering on one side of the helix bundle are indicated in bold. Hydrophobic residues exposed on the other side of the bundle are underlined. (**b**) SAXS allows for study of the 3D structure of proteins in solution. Although this method does not reveal atomic details, its resolution is sufficient to determine the multimeric state and shape of a protein. SAXS analysis yields a scattering pattern (black dots). From this pattern, the radius of gyration $R_g$ of the particle in solution can be derived in two model-independent ways: (i) from the Guinier analysis ($R_g$ = 5.68 ± 0.1 nm), and (ii) through the indirect transform algorithm implemented in the program GNOM (5.59 ± 0.1 nm). The algorithm used in GNOM also provides the maximum diameter $D_m$ of the solute particle (here 18.8 ± 0.2 nm). These experimentally determined $R_g$ and $D_m$ values are substantially larger than those calculated from a monomeric IL-26 structural model ($R_g$ = 1.5 nm; $D_m$ = 5.5 nm), or from dimeric IL-26 models (based on IL-22: $R_g$ = 1.8 nm, $D_m$ = 5.9 nm; based on IL-10: $R_g$ = 2.3 nm, $D_m$ = 7.5 nm), indicating that IL-26 forms multimers in our experimental conditions. (**c**) SAXS data can be used to determine a model-independent *ab initio* shape of the solute particle. For our data, this *ab initio* shape resembled four linearly connected spheres (gray beads obtained by the program DAMMIF). Each sphere has the dimensions of one IL-26 monomer. As illustration, one IL-26 molecule (secondary structure representation, color-ramped from blue: N terminus to red: C terminus) was placed by hand in the *ab initio* SAXS shape. Based on these results, we used the program SASREF to position four IL-26 monomers as a tetramer that best fits the experimental SAXS pattern. The calculated SAXS pattern (red line in **b**, produced with CRYSOL) of the resulting tetramer fitted the experimental data (black dots, **b**) with χ = 0.99. (For a good model, χ values should be close to 1. Values much greater than 1 indicate a poor fit of model to data, and χ values much smaller than 1 indicate over-fitting of the data.) SAXS yields the average size of all solute particles. Hence our analysis does not rule out the presence of minor populations of other multimers (3-mers and 5-mers, for example), which are expected to co-exist in a concentration-dependent equilibrium. Repeat runs of SASREF or DAMMIF (both of which use a Monte Carlo algorithm and simulated annealing, and hence can produce different models for each run) produce linear structures with similar, but not identical, curvature, each of which achieves a comparable χ fit. This observation suggests that IL-26 molecules do not form a rigid rod, and retain some flexibility between protomers. (**d**) Four cysteines are well placed to form disulfide bonds that stabilize the compact helix bundle. The atomic model of IL-26 (colored as in **c**) was obtained by homology modeling.

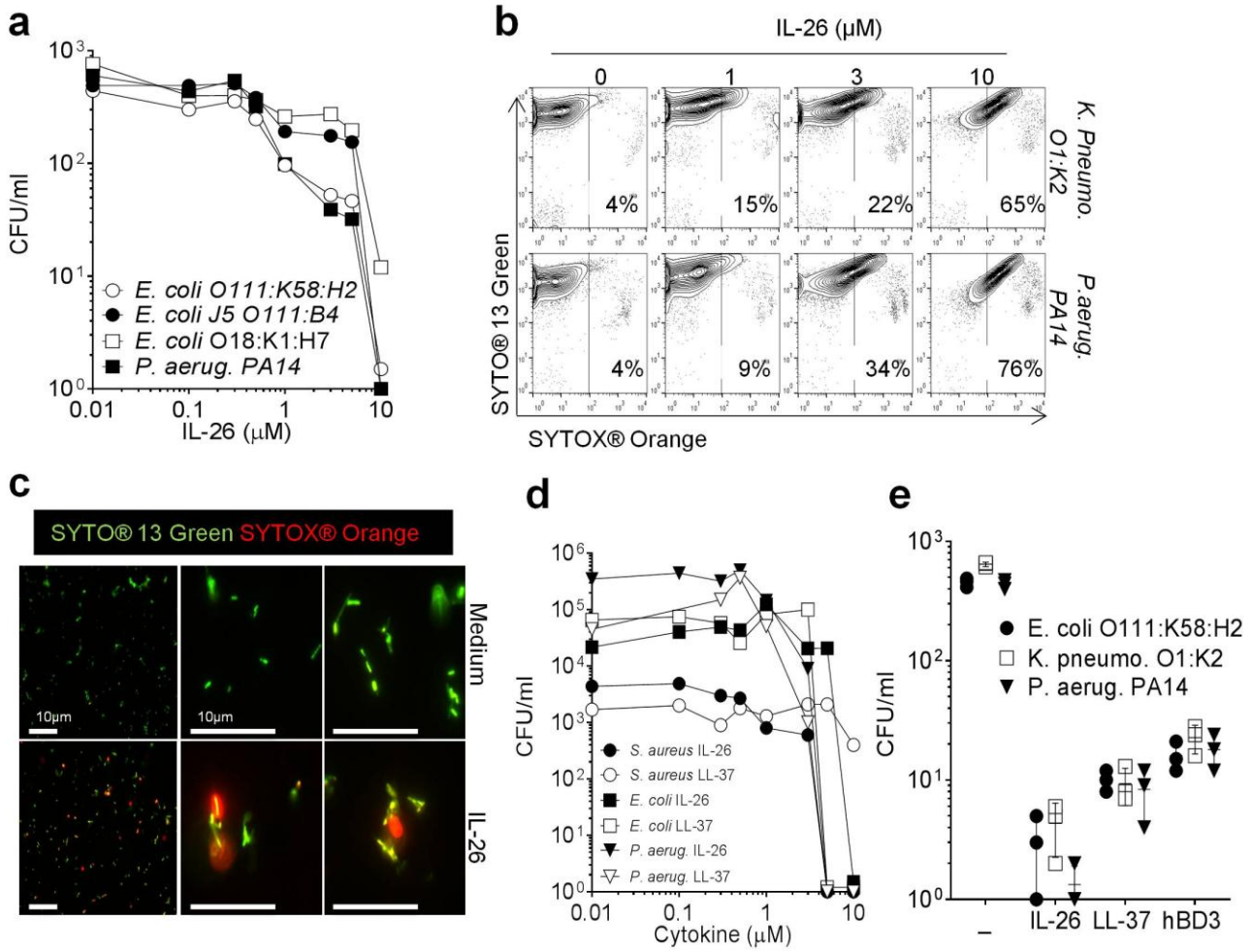


Supplementary Figure 2

**Antimicrobial activity of rhIL-26.**

(**a**) Growth of the virulent strains *E. coli* J5 O111:B4, *E. coli* O111:K58:H2, *E. coli* O18:K1:H7 and *P. aeruginosa* PA14 in culture with increasing concentrations of rhIL-26. (**b**) Flow cytometry analysis of *K. pneumoniae* O1:K2 (top) and *P. aeruginosa* PA14 (bottom) treated with increasing concentrations of rhIL-26 for 1 h and stained with SYTO 13 Green (permeant DNA dye) and SYTOX Orange (impermeant DNA dye). (**c**) Fluorescence microscopy imaging of *K. pneumoniae* O1:K2 in culture medium or treated for 1 h with 10 μM IL-26, and stained with SYTO 13 Green (permeant DNA dye) and SYTOX Orange (impermeant DNA dye). Left images show an overview of the bacteria; middle and right images show bacteria at higher magnification. (**d**) Growth of *S. aureus* ATCC 6538, *E. coli* O1:K1:H7 and *P. aeruginosa* ATCC 27853 in culture with increasing concentrations of rhIL-26 or LL-37. (**e**) Gorwth of *E. coli* O111:K58:H2, *K. pneumoniae* O1:K2 and *P. aeruginosa* PA14 in culture with 10 μM of IL-26, LL-37 or hBD3. **a–e**, Data are representative of three independent experiments. **e**, Error bars represent the s.d. of triplicates.

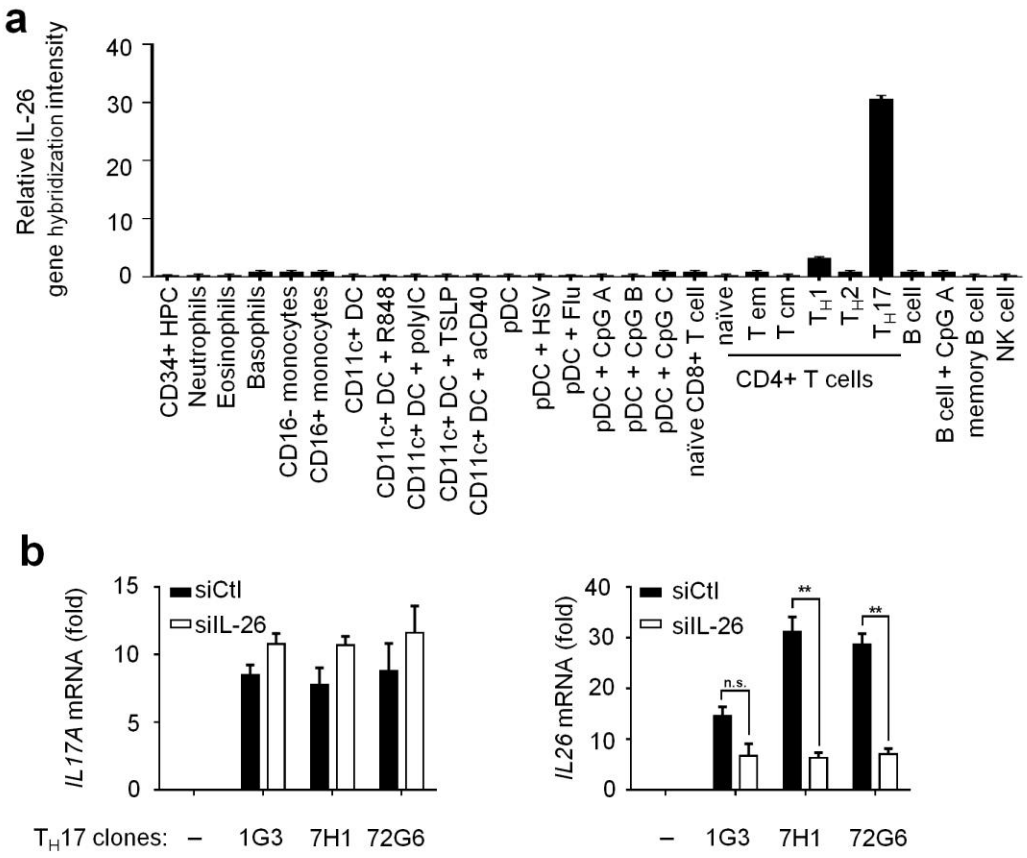


Supplementary Figure 3

**IL-26 is mainly expressed by primary CD4$^+$ $T_H$17 cells and $T_H$17 cell clones.**

(**a**) Microarray gene-expression profile in isolated unstimulated or activated peripheral blood immune cell subsets. $T_H$1, $T_H$2 and $T_H$17 cells were differentiated from naive T cells as described in the Online Methods. The results of the gene-expression profile of IL-26 are shown as the relative hybridization intensity level. Error bars represent the s.d. of duplicates. (**b**) Real-time PCR analysis of *IL17A* and *IL26* mRNA expression in re-stimulated $T_H$17 clones 1G3, 7H1 and 72G6, transfected with siRNA targeting IL-26 (siIL-26) or a control siRNA (siCtl). The feeder cell line LCL was used as a control (-). Error bars are the s.d. of triplicate wells. Data are representative of two independent experiments.

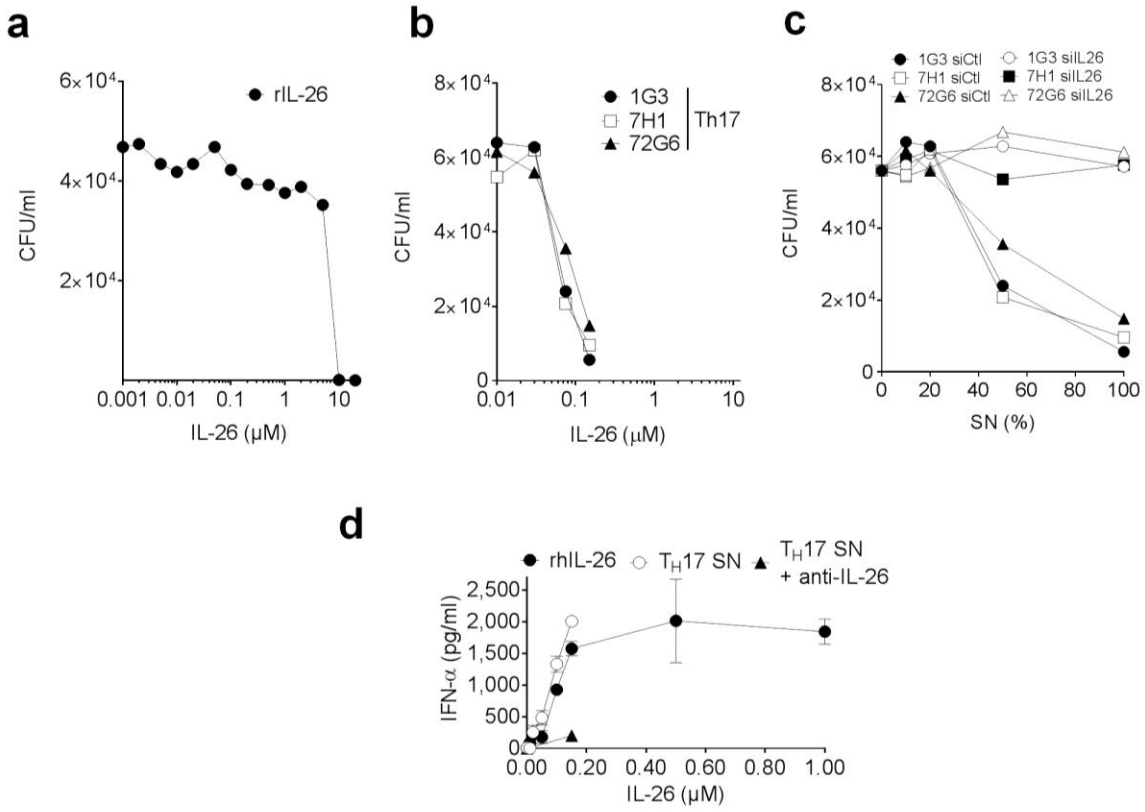


Supplementary Figure 4

**Antimicrobial activity and interferon-inducing capacity of recombinant and natural $T_H17$ cell–derived IL-26.**

(**a**–**c**) Growth of *P. aeruginosa* treated with (**a**) increasing concentrations of rhIL-26, (**b**) supernatants of $T_H17$ cell clones 1G3, 7H1, 72G6 or (**c**) supernatants of $T_H17$ cell clones transfected with siRNA targeting IL-26 (siIL-26) or control siRNA (siCtl). Data are representative of two independent experiments. Data are means of duplicate wells. (**d**) IFN-α produced by pDCs stimulated overnight with exogenous human DNA in the presence of increasing concentrations of rhIL-26, IL-26–containing $T_H17$ cell supernatants, or IL-26–containing $T_H17$ cell supernatants treated with neutralizing anti–IL-26. Error bars represent the standard deviation of duplicate wells. Data are representative of two independent experiments.

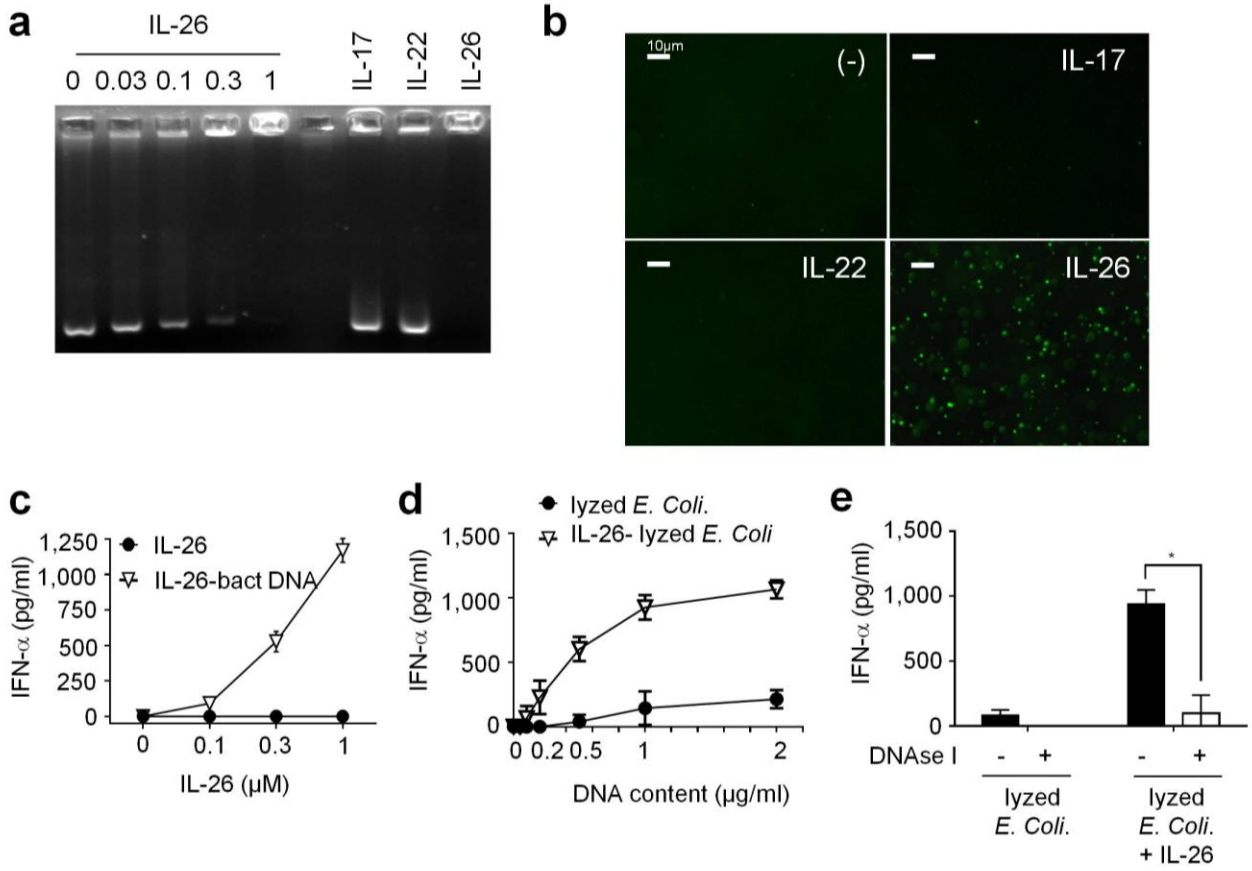


Supplementary Figure 5

**IL-26 forms complexes with bacterial DNA that activate pDCs to produce type I interferon.**

(**a**) Gel shift assay of bactDNA mixed with increasing concentrations of rhIL-26 (left). Mixing with rhIL-17 or IL-22 was used as a control. (**b**) Fluorescence microscopy imaging of Alexa Fluor 488–labeled bactDNA mixed with rhIL-17, rhIL-22 or rhIL-26. (**a**,**b**) Data are representative of two independent experiments. (**c**) IFN-α produced by pDCs stimulated with increasing concentrations of IL-26 either alone or in complex with bactDNA. Data are representative of three independent experiments. Error bars represent the s.d. of duplicate wells. (**d**,**e**) IFN-α produced by pDCs stimulated overnight with (**d**) increasing concentrations of *E. coli* lysate (titrated according to DNA content) in the presence or not of IL-26, (**e**) *E. coli* lysate alone or in the presence of IL-26, with or without DNase pretreatment. **d**,**e**, Data are representative of three independent experiments. Error bars represent the s.d. of triplicate wells. Data in **e** were statistically analyzed via unpaired two-tailed Student's *t*-test; *$P < 0.01$.

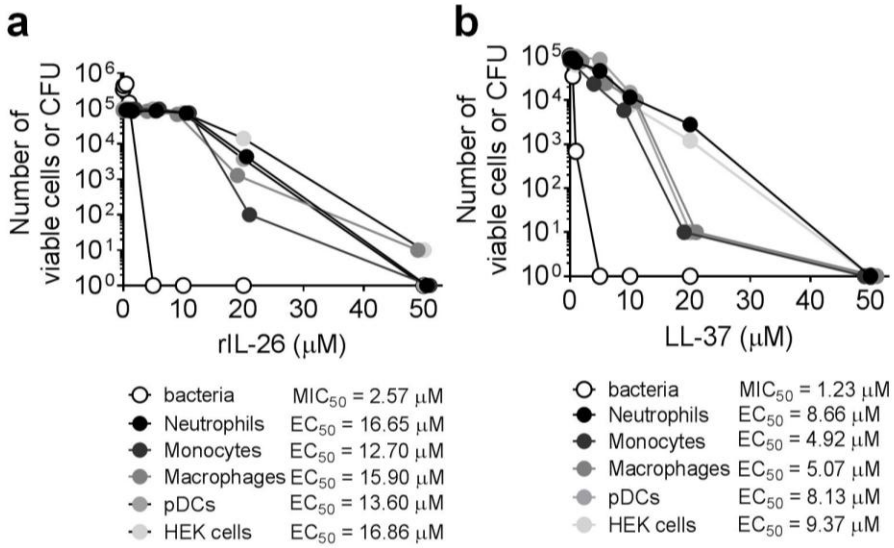


Supplementary Figure 6

**Antimicrobial and cytotoxic activities of rhIL-26 and LL-37.**

Viable bacteria and human neutrophils, monocytes, macrophages, pDCs and HEK cells following overnight culture in the presence of increasing concentrations of rhIL-26 (**a**) or LL-37 (**b**). $MIC_{50}$ for bacteria and $EC_{50}$ for human cells were calculated using nonlinear regression fit curves. Data are representative of two independent experiments. Error bars represent the s.d. of duplicate wells.

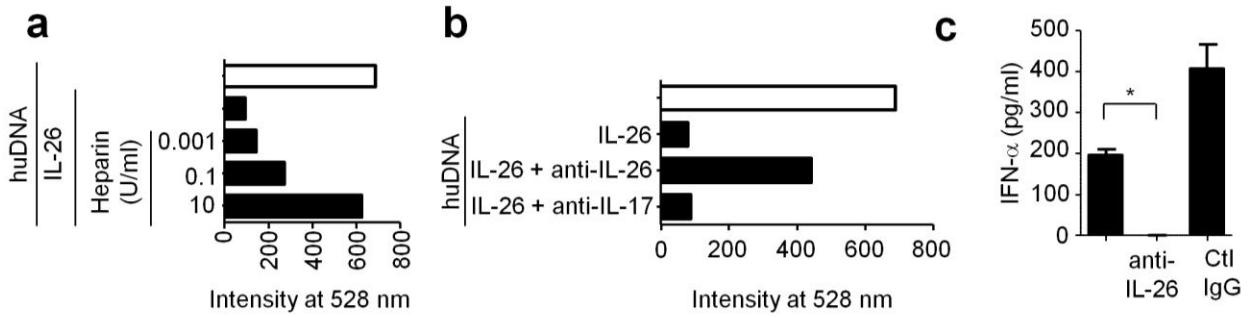


Supplementary Figure 7

**IL-26–human DNA complex formation can be inhibited by anionic polymers and anti–IL-26.**

(**a**,**b**) Fluorimetric quantification of DNA staining by picogreen dye upon mixing of human DNA with IL-26 in the presence of (**a**) increasing concentrations of the anionic polymer heparin or (**b**) neutralizing anti–IL-26 or anti–IL-17. (**c**) IFN-α produced by pDCs stimulated overnight with IL-26–human DNA complexes in the presence of neutralizing anti–IL-26 or isotype control antibodies (ctl IgG). Error bars represent the s.d. of triplicate wells. Data are representative of three independent experiments. Statistical analysis was done using unpaired two-tailed Student's *t*-test; **P* < 0.001.

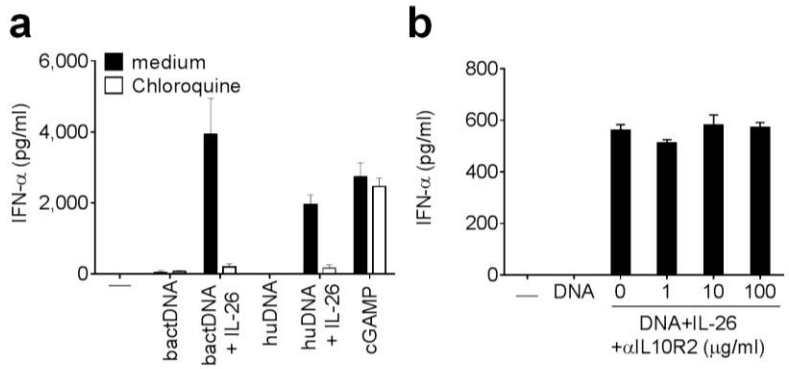


Supplementary Figure 8

**pDC activation by L-26–human DNA is not dependent on the IL-26 receptor and cytosolic DNA sensing.**

(**a**) IFN-α produced by pDCs stimulated overnight with bactDNA or human DNA alone, with IL-26–bactDNA or IL-26–human DNA complexes, or with the STING ligand cGAMP in the presence of 100 ng/ml chloroquine. (**b**) IFN-α produced by pDCs stimulated overnight with human DNA alone or with IL-26–human DNA complexes in the presence of increasing concentrations of blocking antibodies to IL-10R2. Error bars represent the s.d. of triplicate wells. Data are representative of three independent experiments.